



N-end Rule–Mediated Proteasomal Degradation of ATGL Promotes Lipid Storage

Jiesi Xu,¹ Zhenglong Liu,^{1,2} Jianxin Zhang,^{1,2} Siyu Chen,^{1,2} Wei Wang,¹ Xuefan Zhao,^{1,2} Mei Zhen,³ and Xun Huang¹

Diabetes 2023;72:210–222 | <https://doi.org/10.2337/db22-0362>

Cellular lipid storage is regulated by the balance of lipogenesis and lipolysis. The rate-limiting triglyceride hydrolase ATGL (desnutrin/PNPLA2) is critical for lipolysis. The control of ATGL transcription, localization, and activation has been intensively studied, while regulation of the protein stability of ATGL is much less explored. In this study, we showed that the protein stability of ATGL is regulated by the N-end rule in cultured cells and in mice. The N-end rule E3 ligases UBR1 and UBR2 reduce the level of ATGL and affect lipid storage. The N-end rule–resistant ATGL(F2A) mutant, in which the N-terminal phenylalanine (F) of ATGL is substituted by alanine (A), has increased protein stability and enhanced lipolysis activity. *ATGL*^{F2A/F2A} knock-in mice are protected against high-fat diet (HFD)–induced obesity, hepatic steatosis, and insulin resistance. Hepatic knockdown of *Ubr1* attenuates HFD-induced hepatic steatosis by enhancing the ATGL level. Finally, the protein levels of UBR1 and ATGL are negatively correlated in the adipose tissue of obese mice. Our study reveals N-end rule–mediated proteasomal regulation of ATGL, a finding that may potentially be beneficial for treatment of obesity.

Obesity is a major risk factor for common diseases, such as nonalcoholic fatty liver disease, cardiovascular diseases, type 2 diabetes, and some cancers (1). The cause of obesity is complicated and includes factors such as excessive food intake, lack of physical activity, and genetic susceptibility; however, in general, the main reason is excessive lipid storage (2). At the cellular level, the balance of lipogenesis and lipolysis largely determines the lipid storage level. Reduced lipogenesis or elevated lipolysis has often been reported to be protective against the development of obesity and obesity-associated diseases (3,4).

ATGL is a rate-limiting executor of lipolysis, and its level or activity has been associated with various metabolic conditions (5–10). Loss-of-function mutations in human ATGL cause neutral lipid storage disease with myopathy (11). *Atgl*-deficient mice accumulate large amounts of lipid in their hearts, which causes cardiac dysfunction and premature death (12). Interestingly, adipose tissue–specific overexpression or deletion of ATGL appears to be beneficial. Mice with adipose *ATGL* overexpression were protected from diet-induced obesity and showed improved glucose homeostasis (13). Adipose-specific ATGL knockout mice had slightly increased body weight but exhibited improved glucose tolerance and hepatic insulin sensitivity (14). Pharmacological inhibition of ATGL by atglistatin has beneficial effects on high-fat diet (HFD)–induced obesity and hepatic steatosis (15). Therefore, the temporal and spatial regulation of ATGL level or activity appear to be critical for determining the physiological outcome.

ATGL protein is expressed at low levels in nonadipose tissues but is highly expressed in white adipose tissue (WAT) and brown adipose tissue (BAT) (16). Previous studies revealed that ATGL expression/activity can be regulated transcriptionally and posttranscriptionally (17–21). Numerous binding partners of ATGL have also been identified. α/β Hydrolase domain-containing 5 (ABHD5, also named CGI58) is a classic cofactor that directly binds to and activates ATGL (19). In contrast, ATGL activity can be inhibited by GOS2, which physically interacts with the N-terminal patatin domain of ATGL (20). In addition, other ATGL binding partners, such as UBXD8, PEDF, COP1, PEX2, and the Arf1 exchange factor GBF1, may be responsible for modulating

¹State Key Laboratory of Molecular Developmental Biology, Institute of Genetics and Developmental Biology, Chinese Academy of Sciences, Beijing, China

²University of Chinese Academy of Sciences, Beijing, China

³Lunenfeld–Tanebaum Research Institute, Departments of Molecular Genetics and Physiology, University of Toronto, Toronto, Ontario, Canada

Corresponding authors: Jiesi Xu, jxu@genetics.ac.cn, and Xun Huang, xhuang@genetics.ac.cn

Received 14 April 2022 and accepted 3 November 2022

This article contains supplementary material online at <https://doi.org/10.2337/figshare.21502599>.

J.X. and Z.L. contributed equally to this work.

© 2023 by the American Diabetes Association. Readers may use this article as long as the work is properly cited, the use is educational and not for profit, and the work is not altered. More information is available at <https://www.diabetesjournals.org/journals/pages/license>.

the trafficking, localization, or protein level of ATGL (18, 22–25). Despite significant advances in our knowledge of the control of ATGL transcription, localization, and activation, the complete set of in-vivo regulatory events for ATGL is far from clear.

In this study, we found that ATGL protein level is modulated by the N-end rule pathway E3 ligases UBR1 and UBR2. The N-end rule pathway is a proteolytic system in which certain N-terminal residues of short-lived proteins are recognized by a class of ubiquitin ligases to achieve proteasome-mediated degradation (26). We demonstrated that mice with a knock-in of the N-end rule-resistant mutation ATGL(F2A) (designated as *Atgl*^{F2A/F2A}) exhibit elevated lipolysis and are resistant to HFD-induced obesity and hepatic steatosis.

RESEARCH DESIGN AND METHODS

Mice

Atgl^{F2A/F2A} knock-in mice on the C57BL/6 background were generated by Biocytogen Pharmaceuticals Co., Ltd. (Beijing, China). All mice were housed in environmentally controlled conditions (temperature 22°C, 12:12-h light/dark cycle lights on at 0730 h). Male mice were used for all experiments. For HFD feeding, 8-week-old *Atgl*^{+/+} and *Atgl*^{F2A/F2A} mice were housed individually and fed a HFD with 60% kcal fat (D12492; Research Diets, New Brunswick, NJ) for 16 weeks. A glucose tolerance test (GTT) and insulin sensitivity test (ITT) were performed after 16 weeks of HFD feeding. For hepatic knockdown of *Ubr1*, 8-week-old *Atgl*^{+/+} and *Atgl*^{F2A/F2A} mice were injected intravenously with 3×10^{11} genomic copies of AAV-TBG-sh*Con* or AAV-TBG-sh*Ubr1* adeno-associated viruses (AAVs), followed by feeding with a HFD with 60% kcal fat (Research Diets, New Brunswick, NJ) for 8 weeks. All mice were fasted for 5 to 6 h prior to euthanasia, except when otherwise indicated. All animal care and treatment procedures were approved by the Institutional Animal Care and Use Committee.

Cells and Cell Culture

HepG2 cells (no. HB-8065), HeLa cells (no. CCL-2), and 3T3L1 preadipocytes (no. CL-173) were purchased from American Type Culture Collection (Manassas, VA). For transfection, a total of 100 pmol siRNA oligonucleotides was transfected into cells in six-well plates using Lipofectamine 3000 (Invitrogen, Waltham, MA).

Adenoviruses and Adeno-Associated Viruses

The coding sequences of human ATGL and the ATGL(F2A) mutant were amplified by PCR and cloned into the adenovirus vector pADV-mCMV-MCS-3xFlag. Adenovirus was produced by transfection in 293A cells and purified via the cesium chloride gradient centrifugation method. AAV expressing shRNA against mouse *Ubr1* was generated using the AAV vector pAAV-TBG-3Flag-miR30sh*Ubr1*-WPRES. The target sequence is 5'-CCCCTAAGATCCTTCATGA-3'. AAV was produced by transfection into 293T cells and purified

via discontinuous iodixanol gradient (27). Viral genome titers were determined by quantitative RT-PCR.

Statistics

All data are shown as mean \pm SEM, except in Figs. 1D, 2D, and 3H, in which data are shown as violin plots with median. Statistical analyses were performed with the two-tailed, unpaired Student *t* test or ANOVA with post hoc Tukey multiple comparisons test using GraphPad.

Data and Resource Availability

Data sets and resources are available upon request.

RESULTS

Proteasome Activity Is Positively Correlated With Lipid Storage in Worm, Fly, and Mammalian Cells

To find new regulators of neutral lipid storage, we previously performed an RNA interference (RNAi) screen in *Caenorhabditis elegans* (28). We found that two proteasome component genes, *pas-5* and *pbs-4*, caused a decreased lipid storage phenotype when knocked down (Fig. 1A, Supplementary Fig. 1A, and Supplementary Table 1). We then screened other proteasome components through RNAi. Knockdown of nearly all of the core components and a few regulatory components caused a similar reduced lipid storage phenotype (Supplementary Table 1). This suggests a general requirement for the proteasome for proper lipid storage. Meanwhile, in a genetic screen in *Drosophila* (29), we found that overexpression of the proteasome regulatory subunit Rpn2 dramatically increases lipid storage in *Drosophila* third instar salivary gland (Supplementary Fig. 1B). These findings suggest that proteasome activity promotes lipid storage in worms and flies.

We examined the effect of the proteasome inhibitor MG132 on lipid storage in worms and mammalian cells. Compared with the control, MG132 treatment reduced the fat content in worms in a dose-dependent manner (Fig. 1B). Similarly, the size and the number of lipid droplets, as well as triglyceride levels, were all decreased in MG132-treated HepG2 cells (Fig. 1C–F). Together, our results indicate that proteasome activity positively correlates with lipid storage in worm, fly, and mammalian cells.

The ATGL Level Is Regulated by Proteasome Activity

Next, we explored the mechanism underlying the relationship between inhibition of proteasome activity and decreased lipid storage. The proteasome may be involved in the degradation of a negative regulator of lipogenesis or a positive regulator of lipolysis. Previous work showed that the level of ATGL is increased by proteasome inhibitor treatment (18). Therefore, we analyzed the link between proteasome activity, ATGL level, and lipid storage. MG132 treatment greatly increased the endogenous ATGL level in both normal and oleic acid (OA)-loaded cells (Fig. 1G). Interestingly, OA treatment also enhanced the protein levels of ATGL compared with the control (Fig.

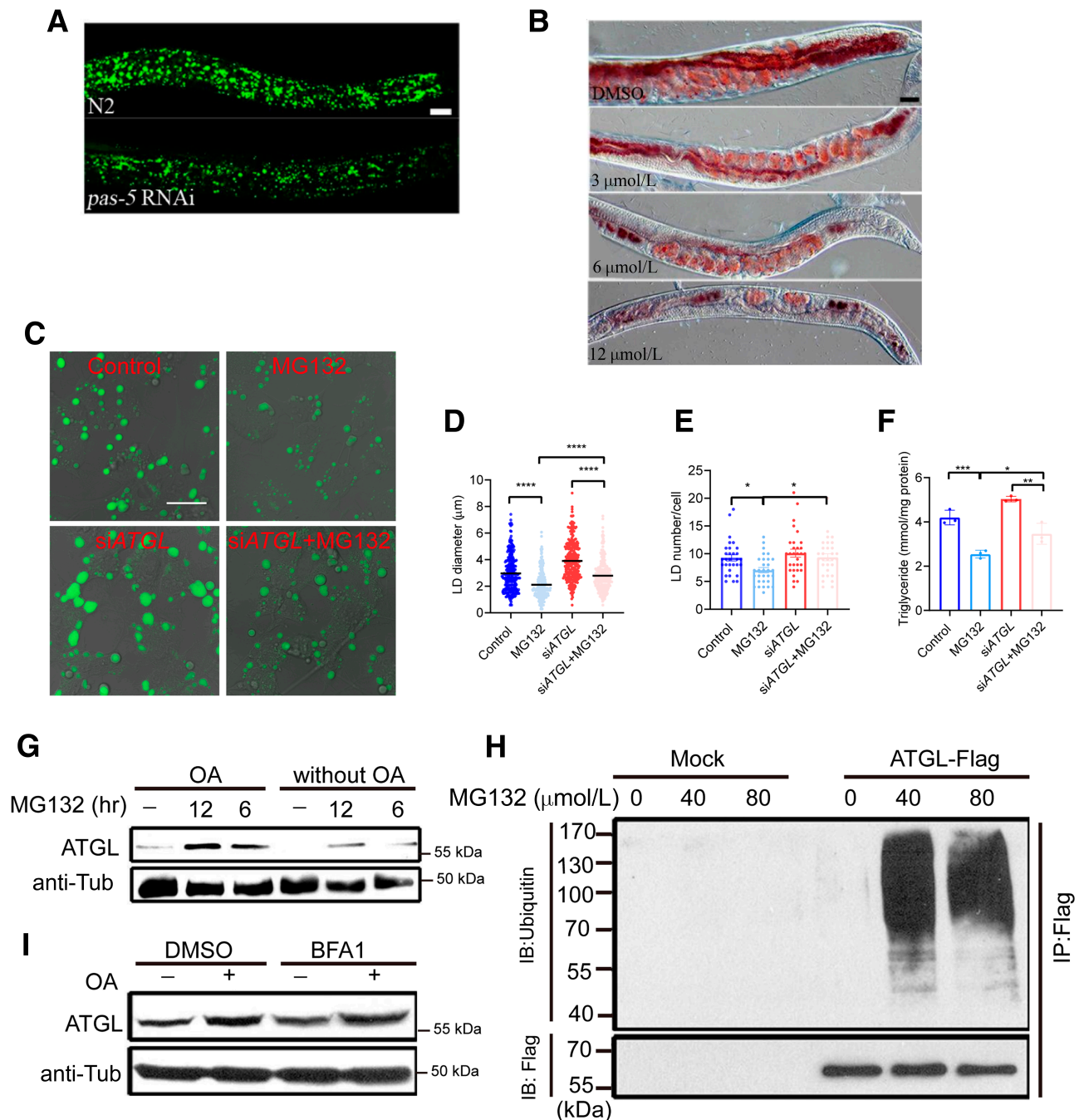


Figure 1—ATGL is degraded through the ubiquitin-proteasome system. **A**: BODIPY staining for lipid droplets in *C. elegans* treated by *pas-5* RNAi compared to the N2 control. Scale bar, 40 μm . **B**: Oil Red O staining for lipid droplets in *C. elegans* treated with the indicated concentration of MG132 for 48 h. Scale bar, 40 μm . **C**: BODIPY staining for lipid droplets in HepG2 cells transfected with siRNA control or siATGL overnight and then treated with 300 $\mu\text{mol/L}$ OA with or without 60 μM MG132 for 24 h. Scale bar, 25 μm . **D**: Quantifications of lipid droplet (LD) sizes in *C. elegans*. $N = 300$ lipid droplets/group. **E**: Quantifications of the number of lipid droplets in *C. elegans*. $N = 50$ cells/group. **F**: Quantifications of triglyceride levels in *C. elegans*. $N = 3$ /group. **G**: Western blot analysis of lysates of HeLa cells treated with or without OA, followed by MG132 treatment for the indicated time. **H**: Western blot analysis of lysates of HeLa cells transfected with mock or ATGL-Flag and treated with MG132 at the indicated concentration. **I**: Western blot analysis of lysates of HeLa cells treated with the lysosome inhibitor bafilomycin A1 (BFA1) under both normal and OA-loaded conditions. All data are presented as mean \pm SEM, except for the violin plots in **D** in which the horizontal lines indicate the median. * $P < 0.05$; ** $P < 0.01$; *** $P < 0.001$; **** $P < 0.0001$. anti-Tub, anti-tubulin; hr, hour; IB, immunoblot; IP, immunoprecipitation.

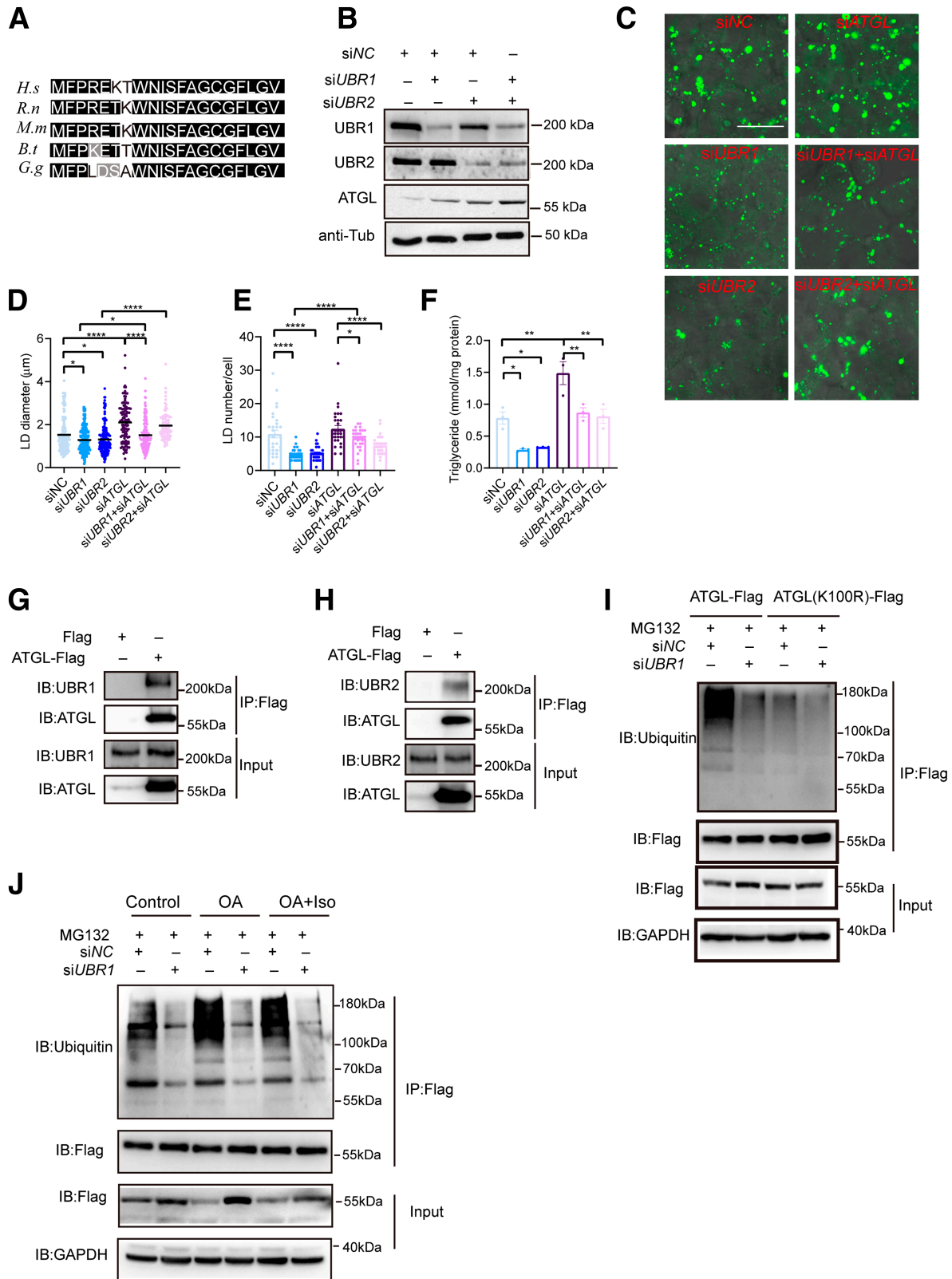


Figure 2—The N-end rule pathway ubiquitin ligases UBR1 and UBR2 regulate ATGL stability and lipid storage in cultured cells. **A**: The conserved destabilizing phenylalanine (F) residue at the N terminus of ATGL (*H.s.*, human; *R.n.*, rat; *M.m.*, mouse; *B.t.*, cattle; and *G.g.*, chicken). **B**: Western blot analysis of proteins in HeLa cells transfected with control siRNA, siUBR1 or siUBR2, or both of the latter for 48 h. **C**: BODIPY staining for lipid droplets in HepG2 cells transfected with control siRNA, siUBR1, siUBR2, siATGL, siUBR1+siATGL, and siUBR2+siATGL and treated with 100 µmol/L OA overnight. Scale bar, 25 µm. **D**: Quantifications of lipid droplet (LD) sizes in **C**. *N* = 300 lipid droplets/group. **E**: Quantifications of the number of lipid droplets in **C**. *N* = 50 cells/group. **F**: Quantifications of triglyceride levels in **C**. *N* = 3/group.

1G). To test whether elevated ATGL is responsible for the MG132-mediated inhibition of lipid storage in OA-loaded cells, we knocked down ATGL in HepG2 cells. The reduced lipid storage caused by MG132 treatment was significantly suppressed by knockdown of ATGL (Fig. 1C–F and Supplementary Fig. 1C).

In agreement with previous findings (18,24), the level of ubiquitinated ATGL was increased upon MG132 treatment (Fig. 1H). In contrast to MG132, treatment with bafilomycin A1, a lysosome H⁺-ATPase inhibitor, did not affect endogenous ATGL levels in cells with or without OA treatment (Fig. 1I). This indicates that ATGL is mainly degraded through the ubiquitin-proteasome pathway. Overall, these data suggest that proteasome activity regulates lipid storage, at least partially, through ATGL degradation.

The N-end Rule Pathway Ubiquitin Ligases UBR1 and UBR2 Affect ATGL Stability and Lipid Storage in Cells

We next sought to identify the E3 ligases that might be responsible for ATGL ubiquitination and degradation. The candidate E3 ligase should fulfill at least two criteria: first, when mutated, it should have a lipid metabolism-related phenotype *in vivo*; and second, it should affect ATGL ubiquitination. Based on these two criteria, we examined the potential involvement of the N-end rule E3 ligase UBR1 (30). UBR is an important component of the N-end rule pathway, and it recognizes and binds to proteins bearing destabilizing N-terminal residues, leading to their ubiquitination and subsequent degradation (31). Importantly, ATGL bears a destabilizing N-end residue, phenylalanine (F), and this residue is conserved in vertebrates (Fig. 2A). In addition, a previous report has shown that *Ubr1*^{-/-} mice exhibit reduced adiposity (30).

We then examined whether the stability of ATGL is regulated by UBR1. *UBR1* RNAi increased the ATGL protein level compared with the negative control (Fig. 2B). Similarly, the endogenous ATGL protein level was increased in HeLa cells with knockdown of *UBR2*, which belongs to UBR protein family and plays redundant roles (31) and was greatly increased in *UBR1/UBR2* double RNAi cells compared with the control (Fig. 2B). Next, we tested whether UBR1 and UBR2 also affect ATGL-mediated lipolysis. ATGL RNAi led to increased lipid storage (Fig. 2C–F). In contrast, knockdown of *UBR1* or *UBR2* reduced the size and number of lipid droplets and lowered the level of triglyceride accumulation in ATGL RNAi HepG2 cells (Fig. 2C–F). This indicates that UBR1 and UBR2 affect ATGL-regulated lipid storage.

We also examined the physical interaction between the proteins. Both UBR1 and UBR2 were associated with ATGL-Flag (Fig. 2G and H). We further determined the lysine residues of ATGL that are ubiquitinated by UBR. Consistent with previous findings that the polyubiquitination signal of ATGL is located at the N terminus of the protein (18,24), the ubiquitination signal was detected in Flag-tagged full-length ATGL and a Flag-tagged N-terminal fragment (amino acids 1–160) (Fig. 2I and Supplementary Fig. 1D). Notably, the ubiquitination signal of both full-length and N-terminal ATGL was considerably decreased upon UBR1 knockdown (Fig. 2I and Supplementary Fig. 1D). We searched for UBR1-dependent ubiquitination sites in the N-terminal patatin domain of ATGL. There are six lysine (K) residues in that region, and UBR1 knockdown increased the ATGL protein level when lysine was mutated to arginine (R) at positions 68, 74, 78, 92, or 135 (Supplementary Fig. 1E–G). However, the protein and polyubiquitination levels of ATGL (K100R) did not respond to UBR1 knockdown (Fig. 2I and Supplementary Fig. 1G), suggesting that K100 is an UBR1-dependent ubiquitination site of ATGL.

Since OA treatment also increased ATGL protein levels (Fig. 1G), we then tested whether OA treatment affected the polyubiquitination levels of ATGL. The polyubiquitination levels of ATGL were slightly increased by treatment with OA or lipolytic inducer (Fig. 2J). Moreover, knockdown of UBR1 increased ATGL protein stability with or without OA treatment. Similar patterns were observed following the knockdown of COP1 and PEX2, two E3 ligases for ATGL, except that knockdown of PEX2 failed to decrease the polyubiquitination level of ATGL upon treatment with lipolytic inducer (Supplementary Fig. 2A and B). This may be due to lipolysis enhancing the protein level of PEX2 (24). In line with this, neither OA treatment nor knockdown of E3 ligases for ATGL significantly affected the polyubiquitination levels of ATGL (K100R) (Supplementary Fig. 2C and D), which provides further evidence that K100 is important for its protein stability. Collectively, these results indicate that the stability of ATGL can be regulated by UBR1 and UBR2.

The N-end Rule Residue Affects the Stability of ATGL

To investigate whether the N-terminal phenylalanine residue of ATGL is important for its stability, we compared the stability of wild-type (WT) ATGL in HeLa cells with two ATGL mutants, ATGL(F2A) and ATGL(F2V), in which the N-terminal destabilizing residue phenylalanine (F) of ATGL was mutated to the stabilizing residue alanine (A) or valine (V). Western blot results showed that the ATGL(F2A) and

Immunoprecipitation (IP) with anti-Flag antibody and Western blot analysis for UBR1 (G), UBR2 (H), and ATGL in HeLa cells transfected with control vector or ATGL-Flag. I: Immunoprecipitation with anti-Flag antibody and Western blot analysis for ubiquitin in HeLa cells transfected with the indicated siRNA and ATGL-Flag or ATGL(K100R)-Flag vector, followed by treatment with MG132. J: Immunoprecipitation with anti-Flag antibody and Western blot analysis for ubiquitin in HeLa cells transfected with the indicated siRNA and ATGL-Flag vector, followed by treatment with or without 100 μmol/L OA for 16 h or with 100 μmol/L OA for 16 h followed by Iso (0.25 mmol/L 3-isobutyl-1-methylxanthine/1 μmol/L isoproterenol) for 8 h. All data are presented as mean ± SEM, except for D (violin plots), in which the horizontal lines indicate the median. **P* < 0.05; ***P* < 0.01; *****P* < 0.0001. anti-Tub, anti-tubulin; IB, immunoblot; NC, normal control.

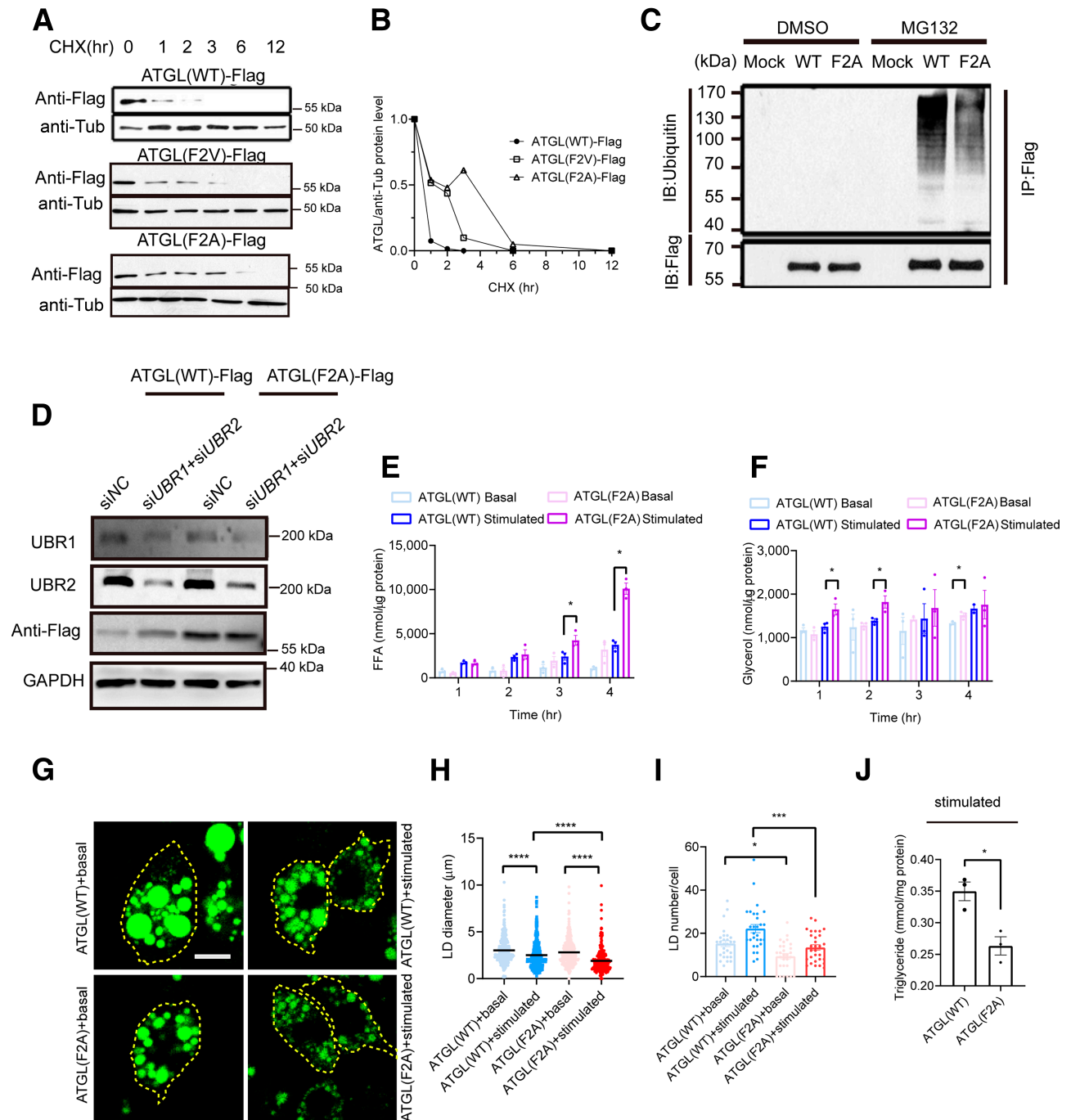


Figure 3—The N-end rule residue affects the stability of ATGL and ATGL-mediated lipolysis. **A**: Western blot analysis of proteins in HeLa cells transfected with ATGL(WT)-Flag, ATGL(F2A)-Flag, or ATGL(F2V)-Flag and treated with 10 $\mu\text{g}/\text{mL}$ cycloheximide (CHX) for the indicated times. **B**: Quantification of relative protein levels in **A**. **C**: Immunoprecipitation (IP) with anti-Flag antibody and Western blot analysis for ubiquitin, and ATGL-Flag in HeLa cells transfected with ATGL(WT)-Flag and ATGL(F2A)-Flag and treated with or without MG132. **D**: Western blot analysis of proteins in HeLa cells stably overexpressing ATGL(WT)-Flag or ATGL(F2A)-Flag and transfected with control siRNA or siUBR1+siUBR2 for 48 h. Release of FFA (**E**) and glycerol (**F**) from differentiated 3T3L1 adipocytes infected with equal amounts of Ad-ATGL(WT)-Flag or Ad-ATGL(F2A)-Flag and treated with or without 10 $\mu\text{mol}/\text{L}$ isoproterenol at 37°C ($N = 3/\text{group}$). **G**: BODIPY staining for lipid droplets in differentiated 3T3L1 adipocytes infected with equal amounts of Ad-ATGL(WT)-Flag or Ad-ATGL(F2A)-Flag and stimulated with or without 10 $\mu\text{mol}/\text{L}$ isoproterenol for 3 h. Adipocytes are outlined with dashed yellow lines. Scale bar, 25 μm . **H**: Quantifications of lipid droplet (LD) sizes in **G**. $N = 300$ lipid droplets/group. **I**: Quantifications of the number of lipid droplets in **G**. $N = 50$ cells/group. **J**: Quantifications of triglyceride levels in **G**. $N = 3/\text{group}$. All data are presented as mean \pm SEM, except for **H**, in which the horizontal lines indicate the median. * $P < 0.05$; *** $P < 0.001$; **** $P < 0.0001$. anti-Tub, anti-tubulin; hr, hour; IB, immunoblot.

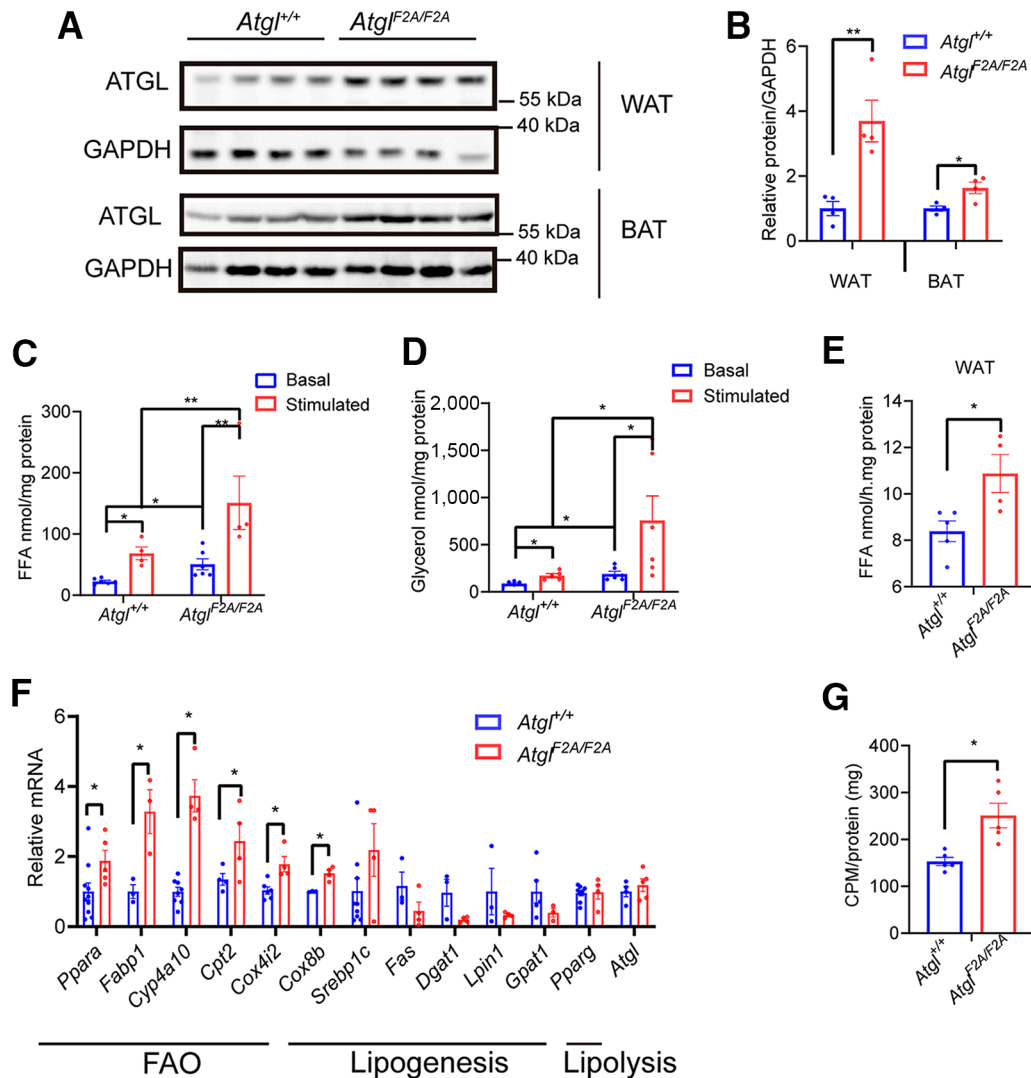


Figure 4—*Atgl*^{F2A/F2A} mice have elevated lipolysis in adipose tissue. **A**: Western blot analysis of proteins in the gonadal WAT or BAT from chow-diet fed *Atgl*^{+/+} and *Atgl*^{F2A/F2A} mice ($N = 4$ mice/group). **B**: Quantification of proteins in **A**. The levels of FFA (**C**) and glycerol (**D**) released from gonadal WAT in chow-diet fed *Atgl*^{+/+} and *Atgl*^{F2A/F2A} mice after overnight fasting ($N = 4$ – 6 mice/group). **E**: Triglyceride hydrolase activity in gonadal WAT from *Atgl*^{+/+} and *Atgl*^{F2A/F2A} mice that were fed a HFD for 8 weeks ($N = 4$ – 5 mice/group). **F**: mRNA levels of genes involved in FAO (**F**) and the activity of FAO (**G**) in gonadal WAT from *Atgl*^{+/+} and *Atgl*^{F2A/F2A} mice, which were fed a HFD for 8 weeks ($N = 3$ – 10 mice/group). All data are presented as mean \pm SEM. * $P < 0.05$; ** $P < 0.01$. CPM, count per minute.

ATGL(F2V) mutants are more stable than ATGL(WT) (Fig. 3A and B). We then explored the contribution of the destabilizing phenylalanine residue to the ubiquitination of ATGL. The level of ubiquitinated ATGL(F2A) was lower than that of ATGL(WT) in the presence of MG132 (Fig. 3C). Furthermore, knockdown of *UBR1* and *UBR2* enhanced the level of ATGL(WT) protein but not the ATGL(F2A) mutant (Fig. 3D). This suggests that the N-terminal phenylalanine residue of ATGL is important for *UBR1*- and *UBR2*-regulated protein stability.

ATGL is highly expressed in adipocytes, and ATGL-mediated lipolysis is essential for providing free fatty acid (FFA) for energy production during fasting (16). We then tested whether the ATGL(F2A) mutant affects lipolysis and lipid storage in 3T3L1 adipocytes. In basal state 3T3L1 adipocytes, levels of lipolysis, assessed by FFA

and glycerol release, were comparable in cells expressing ATGL(WT) and ATGL(F2A), except that glycerol release was increased in ATGL(F2A) cells at 4 h (Fig. 3E and F). Stimulation of lipolysis with isoproterenol led to increased FFA and glycerol release, and this enhancement was greater in ATGL(F2A) cells compared with ATGL(WT) cells (Fig. 3E and F and Supplementary Fig. 2E). The N-end rule residue substitution did not affect the binding of ATGL with CGI58, an activator of ATGL, or with G0S2, an inhibitor of ATGL (Supplementary Fig. 2F and G). Accordingly, lipid droplet size and number and triglyceride accumulation were decreased in stimulated ATGL(F2A)-expressing cells compared with ATGL(WT)-expressing cells (Fig. 3G–J). In sum, the N-end rule residue affects the stability of ATGL and the level of ATGL-mediated lipolysis.

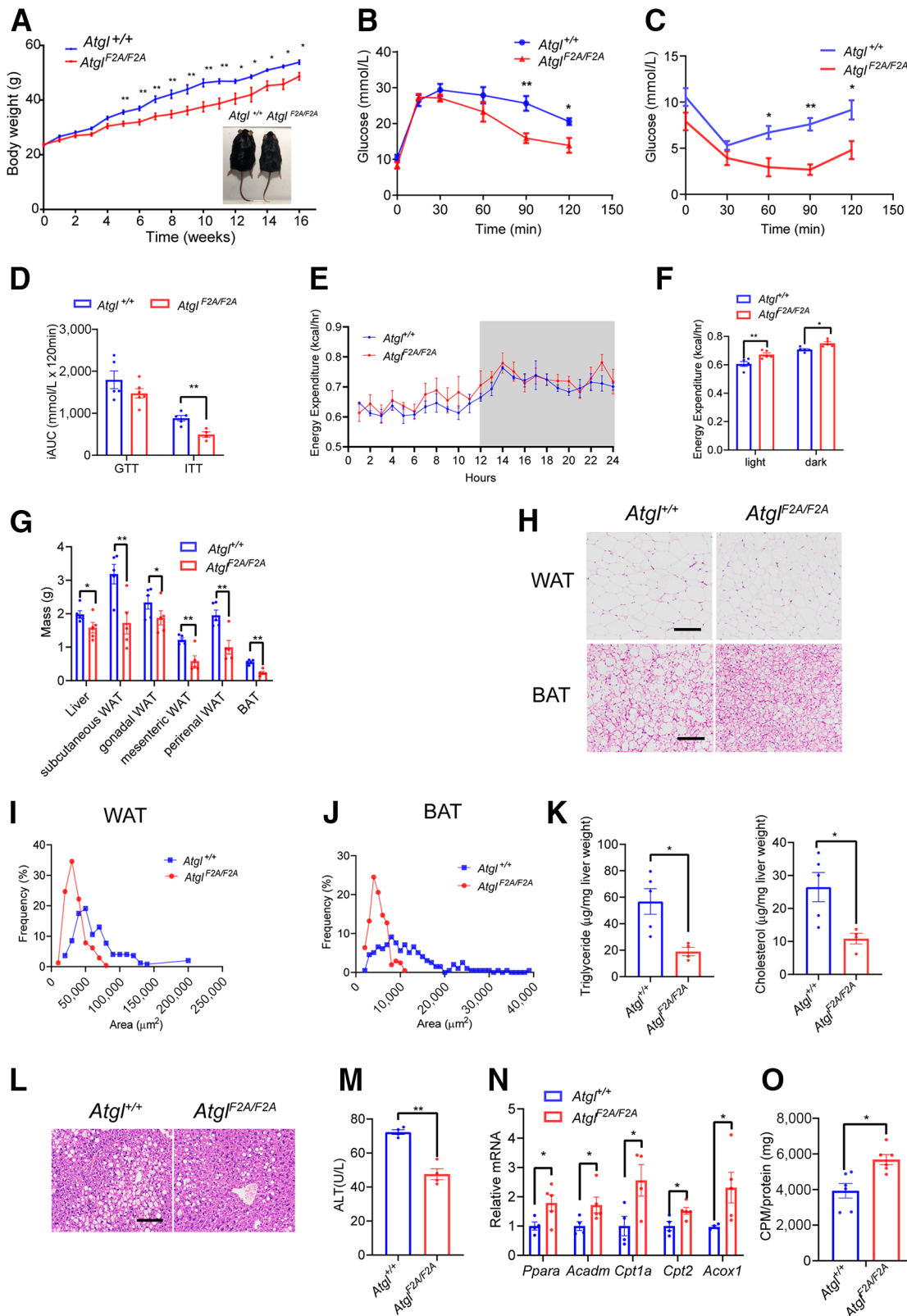


Figure 5—*Atgl*^{F2A/F2A} mice are resistant to diet-induced obesity. **A**: Body weights and images (inset) of 8-week-old *Atgl*^{+/+} and *Atgl*^{F2A/F2A} mice that were pair-fed a HFD for 16 weeks (*N* = 8 mice/group). Results of glucose tolerance (**B**) and insulin sensitivity (**C**) tests after 16 weeks of HFD feeding (*N* = 4–6 mice/group). **D**: Incremental area under the curve (iAUC) of GTT and ITT in **B** and **C**. **E** and **F**: Energy expenditure in HFD-fed mice (*N* = 5 mice/group). **G**: Weights of liver and different fat tissues in HFD-fed mice (*N* = 5 mice/group). Hematoxylin-eosin (H-E) staining of gonadal WAT and BAT sections (**H**) (scale bars, 100 μm) and quantification of adipocyte sizes in WAT (**I**) and BAT (**J**) in HFD-fed mice. **K**: Hepatic triglyceride (left) and total cholesterol levels (right) in HFD-fed mice (*N* = 5 mice/group). **L**: H-E staining of liver sections from

ATGL(F2A) Knock-in Mice Have Elevated Lipolysis and Fatty Acid β -Oxidation in Adipose Tissue

We next sought to reveal the effect of stabilized ATGL in mice. We generated mice with knock-in of the ATGL(F2A) mutation, designated as *Atgl*^{F2A/F2A} (Supplementary Fig. 3A and B). Supplementary Table 2 shows the metabolic profiles of *Atgl*^{+/+} and *Atgl*^{F2A/F2A} mice fed a chow diet.

In gonadal WAT and BAT, the ATGL level was increased 3-fold and 1.5-fold, respectively, in *Atgl*^{F2A/F2A} mice compared with control mice (Fig. 4A and B). Similar to adipose tissue, the ATGL protein level was elevated in muscle from *Atgl*^{F2A/F2A} mice (Supplementary Fig. 3C). Along with the increased protein level, ATGL(F2A) caused enhanced lipolysis *ex vivo* (Fig. 4C and D). When mice were fed a HFD for 8 weeks, ATGL(F2A) led to enhanced FFA release from labeled triglyceride compared with control mice (Fig. 4E).

Previous studies reported that overexpression of ATGL leads to activation of peroxisome proliferator-activated receptor α (PPAR α) signaling and fatty acid β -oxidation (FAO) (32–34). Similarly, expression levels of genes related to PPAR α signaling and FAO were higher in the gonadal WAT from the HFD-fed *Atgl*^{F2A/F2A} mice compared with the control (Fig. 4F). Expression levels of genes involved in lipogenesis and lipolysis were not significantly affected (Fig. 4F). Moreover, direct measurement of FAO using [³H]palmitate showed that FAO was enhanced in the WAT of HFD-fed *Atgl*^{F2A/F2A} mice (Fig. 4G). The development of obesity is associated with stereotypical changes in adipose tissue expression of inflammatory genes. We then examined the adipose inflammation in HFD-fed mice. The adipose inflammation was not significantly affected in HFD-fed *Atgl*^{F2A/F2A} mice (Supplementary Fig. 3D). Overall, these data suggest that *Atgl*^{F2A/F2A} mice have increased levels of ATGL protein and triglyceride hydrolase activity in adipose tissue.

Atgl^{F2A/F2A} Mice Are Resistant to Diet-Induced Obesity and Hepatic Steatosis

Next, we examined the effect of ATGL(F2A) on the development of obesity. *Atgl*^{+/+} and *Atgl*^{F2A/F2A} mice were pair-fed a HFD for 16 weeks starting from 8 weeks of age. We used pair-feeding to ensure similar food intake by these two groups (Supplementary Fig. 3E), because it has been reported that loss of *Atgl* or pharmacological ATGL inhibition affects food intake (15,35). The plasma parameters are shown in Supplementary Table 3.

The body weight gain of *Atgl*^{F2A/F2A} mice was less than that of *Atgl*^{+/+} mice (Fig. 5A). Glucose tolerance and insulin sensitivity were improved in HFD-fed *Atgl*^{F2A/F2A} mice compared with *Atgl*^{+/+} mice (Fig. 5B–D). To determine the effect of ATGL(F2A) on energy balance, we measured oxygen consumption (O₂), carbon dioxide (CO₂) production,

and energy expenditure. These levels were higher in HFD-fed *Atgl*^{F2A/F2A} mice compared with *Atgl*^{+/+} mice (Fig. 5E and F and Supplementary Fig. 3F and G).

The attenuated body weight gain in HFD-fed *Atgl*^{F2A/F2A} mice led us to examine adiposity. The liver weight and the weights of WAT and BAT were decreased in *Atgl*^{F2A/F2A} mice compared with *Atgl*^{+/+} mice when fed a HFD (Fig. 5G and Supplementary Fig. 3H). The sizes of adipocytes in WAT and BAT were also decreased in adipose tissue sections from HFD-fed *Atgl*^{F2A/F2A} mice compared with control mice (Fig. 5H–J).

The reduced liver weight in HFD-fed *Atgl*^{F2A/F2A} mice led us to further analyze the effect of ATGL(F2A) in liver. Hepatic triglyceride and total cholesterol levels and hepatic lipid droplet accumulation were significantly decreased in HFD-fed *Atgl*^{F2A/F2A} mice compared with *Atgl*^{+/+} mice (Fig. 5K and L). The ALT level, which indicates liver damage, was decreased in HFD-fed *Atgl*^{F2A/F2A} mice compared with *Atgl*^{+/+} mice (Fig. 5M). ATGL protein levels were increased in the liver of *Atgl*^{F2A/F2A} mice compared with control mice (Supplementary Fig. 3I). To further determine whether reduced lipid accumulation in the liver of *Atgl*^{F2A/F2A} mice was attributable to enhanced lipid degradation, we measured the FAO level. Expression levels of genes involved in FAO and fatty acid transport were significantly increased (Fig. 5N). The FAO level was significantly enhanced in the liver of HFD-fed *Atgl*^{F2A/F2A} mice compared with control (Fig. 5O). Taken together, these results suggest that *Atgl*^{F2A/F2A} mice, which carry a stabilizing N-terminal amino acid substitution, are resistant to HFD-induced obesity and hepatic steatosis.

Hepatic Knockdown of *Ubr1* Suppresses HFD-Induced Fatty Liver

We then examined the physiological effect of UBR1-mediated ATGL degradation in mice. We knocked down *Ubr-1* (AAV-TBG-sh*Ubr1*) in the liver of *Atgl*^{+/+} or *Atgl*^{F2A/F2A} mice. The thyroxine-binding globulin (TBG) promoter ensures gene knockdown in the liver. Control animals received AAV-TBG-sh*Con*. Hepatic knockdown of *Ubr1* did not affect hepatic triglyceride levels in fed or fasted mice on a chow diet (Supplementary Fig. 4A). We also fed the animals with a HFD for 8 weeks. As expected, HFD-fed *Atgl*^{F2A/F2A} mice showed attenuated body weight gain, less hepatic lipid accumulation, and decreased plasma ALT levels compared with HFD-fed *Atgl*^{+/+} mice (Fig. 6A–C and Supplementary Fig. 4B). These beneficial effects were not affected by hepatic knockdown of *Ubr1* in HFD-fed *Atgl*^{F2A/F2A} mice (Fig. 6A–C and Supplementary Fig. 4B), which suggests that UBR1-mediated ATGL degradation is blunted in *Atgl*^{F2A/F2A} mice. Nevertheless, hepatic knockdown of *Ubr1* caused reductions in hepatic lipid accumulation and

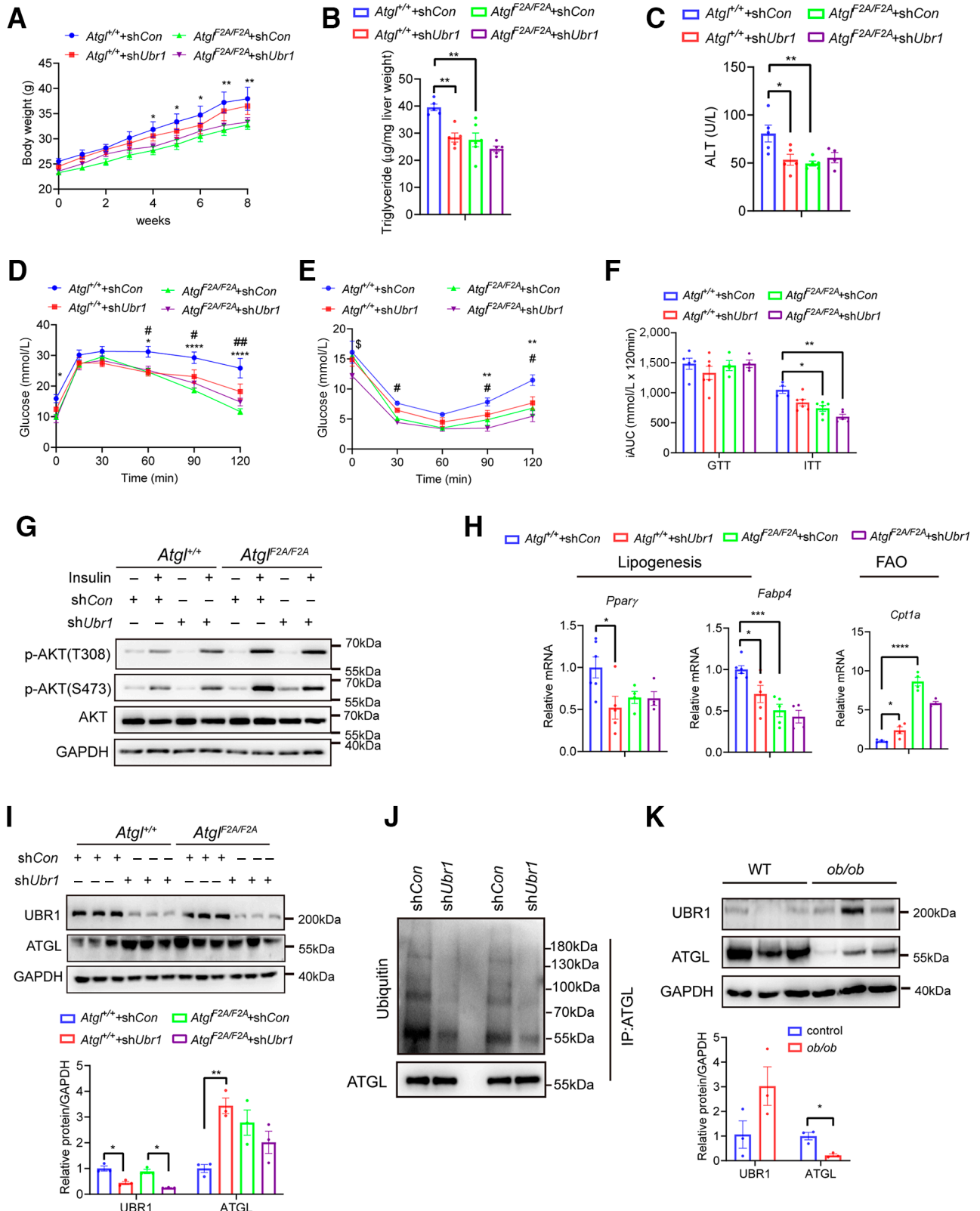


Figure 6—Hepatic knockdown of UBR1 attenuates HFD-induced hepatic steatosis. **A**: Body weights of 8-week-old *Atgl*^{+/+} and *Atgl*^{F2A/F2A} mice injected with AAV-TBG-shCon or AAV-TBG-shUbr1 and fed n HFD for 8 weeks (*N* = 8 mice/group). Hepatic triglyceride levels (**B**) and plasma ALT levels (**C**) in HFD-fed mice (*N* = 5 mice/group). Results of GTT (**D**) and ITT (**E**) in HFD-fed mice (*N* = 5–6 mice/group). **F**: Incremental area under the curve (iAUC) of GTT and ITT in **B** and **C**. **G**: Western blot analysis of proteins from the liver of HFD-fed mice that were fasted for 12 h and injected with 1 unit/kg insulin intraperitoneally. **H**: mRNA levels of genes in the liver of HFD-fed mice (*N* = 4–6 mice/group). **I**: Western blot analysis of proteins in the liver of HFD-fed mice (*N* = 3 mice/group). **J**: Immunoprecipitation (IP) of ATGL and Western blot

plasma ALT levels in HFD-fed *Atgl*^{+/+} mice (Fig. 6A–C and Supplementary Fig. 4B).

We then tested the energy balance and glucose homeostasis in HFD-fed *Atgl*^{+/+} and *Atgl*^{F2A/F2A} mice with or without knockdown of hepatic *Ubr1*. The VO₂, VCO₂, and energy expenditure were significantly enhanced in *Atgl*^{F2A/F2A} mice compared with *Atgl*^{+/+} mice (Supplementary Fig. 4C–E). Knockdown of *Ubr1* did not affect their levels irrespective of genotypes (Supplementary Fig. 4C–E). In line with previous findings, HFD-fed *Atgl*^{F2A/F2A} mice showed improved glucose homeostasis and insulin sensitivity compared with *Atgl*^{+/+} mice (Fig. 6D–F and Supplementary Fig. 4F). Although knockdown of *Ubr1* improved glucose homeostasis in AAV-TBG-sh*Ubr1*-treated *Atgl*^{+/+} mice compared with AAV-TBG-sh*Con*-treated *Atgl*^{+/+} mice, it had no effects on glucose homeostasis in *Atgl*^{F2A/F2A} mice (Fig. 6D–F and Supplementary Fig. 4F). To examine the activity of the insulin pathway, HFD-fed *Atgl*^{+/+} and *Atgl*^{F2A/F2A} mice were injected with 1 unit/kg insulin intraperitoneally. p-AKT (Ser473) and p-AKT(Thr308) levels were enhanced in the liver of *Atgl*^{F2A/F2A} mice compared with *Atgl*^{+/+} mice (Fig. 6G). Importantly, knockdown of hepatic *Ubr1* did not affect the activity of the insulin pathway in the liver of *Atgl*^{F2A/F2A} mice (Fig. 6G). Moreover, knockdown of hepatic *Ubr1* did not affect the activity of the insulin pathway in the muscle and WAT in both genotypes (Supplementary Fig. 4G and H). Taken together, these data suggest that the beneficial effects of the *Atgl*^{F2A} mutation on HFD-induced hepatic steatosis and glucose homeostasis in mice are not affected by knockdown of hepatic *Ubr1*.

Analysis of hepatic gene expression levels showed that *Ubr1* deficiency downregulated the expression of *Pparg* and its target *Fabp4* in *Atgl*^{+/+} mice, but this effect was blunted in *Atgl*^{F2A/F2A} mice (Fig. 6H). A similar pattern was shown by other genes involved in lipogenesis (Supplementary Fig. 4I). The expression levels of genes involved in FAO and lipolysis were enhanced in *Atgl*^{F2A/F2A} mice compared with *Atgl*^{+/+} mice (Fig. 6H and Supplementary Fig. 4I). Knockdown of *Ubr1* also increased the expression levels of FAO genes in *Atgl*^{+/+} mice, but it caused no further upregulation of these genes in *Atgl*^{F2A/F2A} mice (Fig. 6H and Supplementary Fig. 4I). Next, we tested whether UBR1 regulates ATGL levels in vivo. ATGL protein levels were elevated by knockdown of *Ubr1* in *Atgl*^{+/+} mice and were not affected by knockdown of *Ubr1* in *Atgl*^{F2A/F2A} mice (Fig. 6I). Accordingly, the polyubiquitination levels of ATGL were lowered by knockdown of hepatic *Ubr1* in *Atgl*^{+/+} mice (Fig. 6J). PNPLA3 and PNPLA4, which are PNPLA family members, also contain N-terminal destabilized residues. PNPLA4, but not PNPLA3, was regulated by UBR1 in HeLa cells (Supplementary Fig. 4J and K). Together, these data suggest that in the HFD

condition, hepatic knockdown of *Ubr1* reduces lipogenesis and increases FAO. Moreover, the phenotypic similarity of *Atgl*^{F2A/F2A} mice with or without *Ubr1* knockdown indicates that the N-end rule-mediated degradation of ATGL by UBR1 occurs in vivo.

We further examined the correlation between UBR1 and ATGL levels in obese mice. Consistent with previous reports (36), ATGL protein levels were downregulated in *ob/ob* mice. Interestingly, UBR1 levels were upregulated in *ob/ob* mice, which suggests a negative correlation between UBR1 and ATGL levels (Fig. 6K). Together, these results demonstrate that the N-end rule-mediated proteasomal degradation of ATGL regulates hepatic lipid metabolism and insulin sensitivity.

DISCUSSION

In this study, we found that ATGL, which possesses a typical destabilizing N-terminal residue, is regulated through the N-end rule pathway. Knockdown of the E3 ligases UBR1 and UBR2, or treatment with a proteasome inhibitor, elevates the ATGL level and reduces lipid storage. Importantly, stabilized ATGL [ATGL(F2A)] has beneficial effects on HFD-induced obesity and associated hepatic steatosis in mice.

The N-end Rule UBR Ligase Regulates Lipid Storage Through ATGL

Based on our results and previous findings (18,24), inhibition of proteasome activity or RNAi of proteasome components results in reduced lipid storage in *C. elegans*, *Drosophila*, and cultured mammalian cells. The proteasomal regulation of lipid storage occurs at least partially through ATGL degradation. Previous studies on ATGL protein levels used N-terminal tagged ATGL, thus possibly masking the N-end rule regulation of this protein (18,25). The N-end rule regulation of ATGL is apparently not the only mechanism that regulates ubiquitination or degradation of ATGL because the ATGL(F2A) protein can still be ubiquitinated (Fig. 3C). E3 ubiquitin ligase COP1 and PEX2 also target ATGL for proteasomal degradation (18,24).

Our study showed that knockdown of UBR or treatment with proteasome inhibitor can reduce lipid storage in the absence of ATGL in OA-loaded HepG2 cells (Figs. 1C–F and 2C–F). This suggests that other factors involved in lipolysis or lipogenesis can also be involved in UBR1- or proteasome inhibitor-mediated lipid metabolism. In fact, UBR1 has been shown to degrade lipid droplet proteins in yeast (37). A recent study identified PLIN2 as a substrate of UBR1 in mice (38).

analysis of polyubiquitination levels of ATGL in liver lysates from *Atgl*^{+/+} mice infected with AAV-TBG-sh*Con* or AAV-TBG-sh*Ubr1* Results from two sh*Con*- and two sh*Ubr1*-treated mice are shown. K: Western blot detection of ATGL and UBR1 in the adipose tissue of 8-week-old C57BL/6 or *ob/ob* mice (N = 3 mice/group). *P < 0.05; **P < 0.01; ***P < 0.001; ****P < 0.0001. For E and F, * represents *Atgl*^{+/+} + sh*Con* vs. *Atgl*^{F2A/F2A} + sh*Con*; # represents *Atgl*^{+/+} + sh*Con* vs. *Atgl*^{+/+} + sh*Ubr1*; \$ represents *Atgl*^{F2A/F2A} + sh*Con* vs. *Atgl*^{F2A/F2A} + sh*Ubr1*.

Beneficial Effects of *Atgl*^{F2A/F2A}

The *Atgl*^{F2A/F2A} mice reported in this study presumably represent a whole-body gain of function of ATGL. These mice also provide us with an opportunity to study the relationship between ATGL protein stability and organismal physiological function. *Atgl*^{F2A/F2A} mice show improved GTT and ITT results, elevated energy expenditure when fed a HFD, and resistance to HFD-induced obesity and hepatic steatosis. These beneficial effects appear similar to those in *GOS2*^{-/-} and adipose-specific ATGL overexpression (*ap2-desnutrin*) mice (13,39). The common features among these mouse models are elevated lipolysis in adipose tissue and reduced triglyceride accumulation in liver upon HFD feeding.

The elevated flux of fatty acids from adipose tissue can result in triglyceride accumulation in other peripheral tissues, such as liver. The decreased triglyceride accumulation in the liver of HFD-fed *Atgl*^{F2A/F2A} mice may be due to decreased FFA release from adipose tissue or increased triglyceride degradation in liver. Although the ATGL level is apparently enhanced in the adipose tissue of *Atgl*^{F2A/F2A} mice, the change of plasma FFA level is modest upon HFD feeding (Fig. 4A and Supplementary Table 3). The enhanced FAO and PPAR α signaling in the adipose tissue of *Atgl*^{F2A/F2A} mice may dampen the FFA release from adipose tissue (Fig. 4F and G). Similarly, plasma FFA levels were only slightly higher in *ap2-desnutrin* mice compared with control mice, which was in part due to elevated FAO within adipose tissue (13). In contrast, elevated hepatic ATGL levels and enhanced FAO in the liver of *Atgl*^{F2A/F2A} mice may account for attenuated HFD-induced hepatic steatosis. In addition, enhanced energy expenditure, improved insulin sensitivity, and attenuated HFD-induced body weight gain may also contribute to the beneficial effect in the liver.

Glucose tolerance and insulin sensitivity are improved in HFD-fed *Atgl*^{F2A/F2A} mice. It has been reported that lipotoxicity is a causal factor for insulin resistance. It is plausible that reduced lipid accumulation in liver and decreased adiposity relieve the burden of HFD-induced lipid overload, thus improving glucose tolerance and insulin sensitivity. In line with that, both *GOS2*^{-/-} and *ap2-desnutrin* mice showed improved glucose homeostasis upon HFD feeding. Notably, the beneficial effect in *GOS2*^{-/-} and *Atgl*^{F2A/F2A} mice results from the action of ATGL in both liver and adipose tissue, while the beneficial effect in *ap2-desnutrin* mice is predominantly due to the action of ATGL in adipose tissue. We have observed that knockdown of hepatic *Ubr1* improved the activity of the insulin pathway (Fig. 6D–G). UBR1 may directly regulate components of the insulin signaling pathway. Alternatively, it may regulate hepatic lipids, such as diacylglycerol or ceramide, which in turn affect hepatic insulin signaling.

Both Loss of Function and Gain of Function of ATGL Can Yield Beneficial Physiological Outcomes

ATGL apparently has dual effects on metabolism and physiology. Tissue-specific knockout or overexpression of ATGL appears to have beneficial effects on glucose metabolism in

mice (13,14,40). In humans, both whole-body loss of function and gain of function of ATGL result in deleterious effects. On one hand, loss of ATGL results in neutral lipid storage disease with life-threatening myopathy (11). On the other hand, gain of ATGL function in patients with a C-terminal mutation in PLIN1 is associated with a dominant partial lipodystrophy with severe dyslipidemia and insulin resistance (41). We cannot rule out the possibility that the deleterious effects in patients with the PLIN1 C-terminal truncation could be caused by a combination of both gain of function of ATGL and partial loss of function of PLIN1. Nevertheless, these results indicate that maintaining a suitable level of ATGL in vivo appears to be essential for sustaining healthy physiological conditions in humans. In summary, our findings suggest that the level and the site of ATGL upregulation are probably critical to determining the outcomes of ATGL manipulation.

Acknowledgments. The authors thank Drs. H. Yang (University of New South Wales), J. Liu (Mayo Clinic), C. Yang (Yunnan University), and J. Speakman, S. Bao, and Z. Xu (Institute of Genetics and Developmental Biology, Chinese Academy of Sciences) for providing reagents and helpful discussions.

Funding. This research was supported by the National Natural Science Foundation of China grants 32230044 and 91954207, and the Ministry of Science and Technology of China grant 2018YFA0506902.

Duality of Interest. No potential conflicts of interest relevant to this article were reported.

Author Contributions. J.X., Z.L., J.Z., S.C., and W.W. conducted the experiments and analyzed the data. Z.L. contributed to *C. elegans* experiments. J.X. and Z.L. contributed to cell experiments. J.X., Z.L., J.Z., S.C., and X.Z. contributed to mouse experiments. W.W. contributed to Western blotting. M.Z. contributed to the identification of UBR1. J.X., Z.L., and X.H. wrote the article. X.H. is the guarantor of this work and, as such, had full access to all of the data in the study and takes responsibility for the integrity of the data and the accuracy of the data analysis.

References

1. Tiniakos DG, Vos MB, Brunt EM. Nonalcoholic fatty liver disease: pathology and pathogenesis. *Annu Rev Pathol* 2010;5:145–171
2. Adams JP, Murphy PG. Obesity in anaesthesia and intensive care. *Br J Anaesth* 2000;85:91–108
3. Li JJ, Ferry RJ Jr, Diao S, Xue B, Bahouth SW, Liao FF. Nedd4 haploinsufficient mice display moderate insulin resistance, enhanced lipolysis, and protection against high-fat diet-induced obesity. *Endocrinology* 2015;156:1283–1291
4. Lodhi IJ, Yin L, Jensen-Urstad APL, et al. Inhibiting adipose tissue lipogenesis reprograms thermogenesis and PPAR γ activation to decrease diet-induced obesity. *Cell Metab* 2012;16:189–201
5. Jenkins CM, Mancuso DJ, Yan W, Sims HF, Gibson B, Gross RW. Identification, cloning, expression, and purification of three novel human calcium-independent phospholipase A2 family members possessing triacylglycerol lipase and acylglycerol transacylase activities. *J Biol Chem* 2004;279:48968–48975
6. Villena JA, Roy S, Sarkadi-Nagy E, Kim KH, Sul HS. Desnutrin, an adipocyte gene encoding a novel patatin domain-containing protein, is induced by fasting and glucocorticoids: ectopic expression of desnutrin increases triglyceride hydrolysis. *J Biol Chem* 2004;279:47066–47075
7. Zimmermann R, Strauss JG, Haemmerle G, et al. Fat mobilization in adipose tissue is promoted by adipose triglyceride lipase. *Science* 2004;306:1383–1386

8. Kienesberger PC, Puliniikunnil T, Nagendran J, et al. Early structural and metabolic cardiac remodelling in response to inducible adipose triglyceride lipase ablation. *Cardiovasc Res* 2013;99:442–451
9. Kienesberger PC, Puliniikunnil T, Sung MMY, et al. Myocardial ATGL overexpression decreases the reliance on fatty acid oxidation and protects against pressure overload-induced cardiac dysfunction. *Mol Cell Biol* 2012;32:740–750
10. Wu JW, Wang SP, Alvarez F, et al. Deficiency of liver adipose triglyceride lipase in mice causes progressive hepatic steatosis. *Hepatology* 2011;54:122–132
11. Fischer J, Lefèvre C, Morava E, et al. The gene encoding adipose triglyceride lipase (PNPLA2) is mutated in neutral lipid storage disease with myopathy. *Nat Genet* 2007;39:28–30
12. Haemmerle G, Lass A, Zimmermann R, et al. Defective lipolysis and altered energy metabolism in mice lacking adipose triglyceride lipase. *Science* 2006;312:734–737
13. Ahmadian M, Duncan RE, Varady KA, et al. Adipose overexpression of desnutrin promotes fatty acid use and attenuates diet-induced obesity. *Diabetes* 2009;58:855–866
14. Schoiswohl G, Stefanovic-Racic M, Menke MN, et al. Impact of reduced ATGL-mediated adipocyte lipolysis on obesity-associated insulin resistance and inflammation in male mice. *Endocrinology* 2015;156:3610–3624
15. Schweiger M, Romauch M, Schreiber R, et al. Pharmacological inhibition of adipose triglyceride lipase corrects high-fat diet-induced insulin resistance and hepatosteatosis in mice. *Nat Commun* 2017;8:14859
16. Schreiber R, Xie H, Schweiger M. Of mice and men: the physiological role of adipose triglyceride lipase (ATGL). *Biochim Biophys Acta Mol Cell Biol Lipids* 2019;1864:880–899
17. Ahmadian M, Abbott MJ, Tang T, et al. Desnutrin/ATGL is regulated by AMPK and is required for a brown adipose phenotype. *Cell Metab* 2011;13:739–748
18. Ghosh M, Niyogi S, Bhattacharyya M, et al. Ubiquitin ligase COP1 controls hepatic fat metabolism by targeting ATGL for degradation. *Diabetes* 2016;65:3561–3572
19. Lass A, Zimmermann R, Haemmerle G, et al. Adipose triglyceride lipase-mediated lipolysis of cellular fat stores is activated by CGI-58 and defective in Chanarin-Dorfman syndrome. *Cell Metab* 2006;3:309–319
20. Yang X, Lu X, Lombès M, et al. The G(0)/G(1) switch gene 2 regulates adipose lipolysis through association with adipose triglyceride lipase. *Cell Metab* 2010;11:194–205
21. Roy D, Farabaugh KT, Wu J, et al. Coordinated transcriptional control of adipocyte triglyceride lipase (*Atgl*) by transcription factors Sp1 and peroxisome proliferator-activated receptor γ (PPAR γ) during adipocyte differentiation. *J Biol Chem* 2017;292:14827–14835
22. Ellong EN, Soni KG, Bui QT, Sougrat R, Golinelli-Cohen MP, Jackson CL. Interaction between the triglyceride lipase ATGL and the Arf1 activator GBF1. *PLoS One* 2011;6:e21889
23. Olzmann JA, Richter CM, Kopito RR. Spatial regulation of UBXD8 and p97/VCP controls ATGL-mediated lipid droplet turnover. *Proc Natl Acad Sci USA* 2013;110:1345–1350
24. Ding L, Sun W, Balaz M, et al. Peroxisomal β -oxidation acts as a sensor for intracellular fatty acids and regulates lipolysis. *Nat Metab* 2021;3:1648–1661
25. Niyogi S, Ghosh M, Adak M, Chakrabarti P. PEDF promotes nuclear degradation of ATGL through COP1. *Biochem Biophys Res Commun* 2019;512:806–811
26. Bachmair A, Finley D, Varshavsky A. In vivo half-life of a protein is a function of its amino-terminal residue. *Science* 1986;234:179–186
27. Zolotukhin S, Byrne BJ, Mason E, et al. Recombinant adeno-associated virus purification using novel methods improves infectious titer and yield. *Gene Ther* 1999;6:973–985
28. Liu Z, Li X, Ge Q, Ding M, Huang X. A lipid droplet-associated GFP reporter-based screen identifies new fat storage regulators in *C. elegans*. *J Genet Genomics* 2014;41:305–313
29. Yao Y, Li X, Wang W, et al. MRT, functioning with NURF complex, regulates lipid droplet size. *Cell Rep* 2018;24:2972–2984
30. Kwon YT, Xia Z, Davydov IV, Lecker SH, Varshavsky A. Construction and analysis of mouse strains lacking the ubiquitin ligase UBR1 (E3 α) of the N-end rule pathway. *Mol Cell Biol* 2001;21:8007–8021
31. Tasaki T, Sriram SM, Park KS, Kwon YT. The N-end rule pathway. *Annu Rev Biochem* 2012;81:261–289
32. Ong KT, Mashek MT, Bu SY, Greenberg AS, Mashek DG. Adipose triglyceride lipase is a major hepatic lipase that regulates triacylglycerol turnover and fatty acid signaling and partitioning. *Hepatology* 2011;53:116–126
33. Haemmerle G, Moustafa T, Woelkart G, et al. ATGL-mediated fat catabolism regulates cardiac mitochondrial function via PPAR- α and PGC-1. *Nat Med* 2011;17:1076–1085
34. Reid BN, Ables GP, Otlivanchik OA, et al. Hepatic overexpression of hormone-sensitive lipase and adipose triglyceride lipase promotes fatty acid oxidation, stimulates direct release of free fatty acids, and ameliorates steatosis. *J Biol Chem* 2008;283:13087–13099
35. Wu JW, Wang SP, Casavant S, Moreau A, Yang GS, Mitchell GA. Fasting energy homeostasis in mice with adipose deficiency of desnutrin/adipose triglyceride lipase. *Endocrinology* 2012;153:2198–2207
36. Kuang J, Zhang Y, Liu Q, et al. Fat-specific Sirt6 ablation sensitizes mice to high-fat diet-induced obesity and insulin resistance by inhibiting lipolysis. *Diabetes* 2017;66:1159–1171
37. Ruggiano A, Mora G, Buxó L, Carvalho P. Spatial control of lipid droplet proteins by the ERAD ubiquitin ligase Doa10. *EMBO J* 2016;35:1644–1655
38. Zhang Y, Lin S, Peng J, et al. Amelioration of hepatic steatosis by dietary essential amino acid-induced ubiquitination. *Mol Cell* 2022;82:1528–1542.e10
39. Zhang X, Xie X, Heckmann BL, Saarinen AM, Czyzyk TA, Liu J. Targeted disruption of G0/G1 switch gene 2 enhances adipose lipolysis, alters hepatic energy balance, and alleviates high-fat diet-induced liver steatosis. *Diabetes* 2014;63:934–946
40. Schreiber R, Hofer P, Taschler U, et al. Hypophagia and metabolic adaptations in mice with defective ATGL-mediated lipolysis cause resistance to HFD-induced obesity. *Proc Natl Acad Sci USA* 2015;112:13850–13855
41. Gandotra S, Le Dour C, Bottomley W, et al. Perilipin deficiency and autosomal dominant partial lipodystrophy. *N Engl J Med* 2011;364:740–748